

## Sub-20 fs pulse generation from the mirror dispersion controlled Cr:LiSGaF and Cr:LiSAF lasers

I.T. Sorokina<sup>1</sup>, E. Sorokin<sup>1</sup>, E. Wintner<sup>1</sup>, A. Cassanho<sup>2</sup>, H.P. Jenssen<sup>3</sup>, R. Szipőcs<sup>4</sup>

<sup>1</sup>Technische Universität Wien, Abt. Quantenelektronik und Lasertechnik, Gusshausstr. 27/359, A-1040 Wien, Austria

<sup>2</sup>VLOC, Division of II-VI Incorporated, 431 E. Spruce str., Tarpon Springs, Florida 34689, USA

<sup>3</sup>University of Central Florida, CREOL, 12424 Research Parkway, Suite 400, Orlando, Florida 32826, USA

<sup>4</sup>Research Institute for Solid State Physics, P.O. Box 49, H-1525 Budapest, Hungary

Received: 21 March 1997/Revised Version: 9 May 1997

**Abstract.** We describe the state of the art of mirror-dispersion-controlled (MDC) Kerr-lens mode-locked (KLM) Cr:LiSGaF and Cr:LiSAF lasers. Such lasers, in comparison to their prism-controlled forerunners, are distinguished by high reproducibility, stability, and quality of the pulses, as well as compactness of the cavity. The shortest pulses of  $\sim 18$  fs duration and nearly bandwidth-limited quality ( $\Delta\tau\Delta\nu = 0.33$ ) have been produced in Cr:LiSGaF lasers, which have an average output power of 100 mW. In both lasers, krypton-laser was used as an ideal pump source. The effect of a red-shift of the operating wavelength (from 850 to 880 nm) when shortening of the pulse width (from  $\sim 50$  fs to  $\sim 20$  fs) has been observed and discussed.

**PACS:** 42.55.Rz; 42.60.Mi; 42.65.Re

The last decade has been marked by the rapid development of femtosecond solid-state laser technology. The discovery of Kerr-lens mode-locking (KLM) [1], coupled with advances in high-power diode laser arrays, paved the way to compact all-solid-state femtosecond lasers, which have the advantage of low cost, high stability, and robustness. Most of the progress achieved in generation of ultimately short pulses has been made with KLM Ti:sapphire, pumped either by an Ar-laser or a frequency-doubled neodymium laser. However, the only major shortcoming of Ti:sapphire which has absorption in the blue-green spectral region, is the fact that it still cannot be directly diode-pumped due to the absence of sufficiently powerful blue-green semiconductor lasers at the present time. Therefore, Cr<sup>3+</sup>-doped colquiriite crystals, such as Cr:LiSGaF [2, 3] and Cr:LiSAF [4] which possess absorption bands that overlap the wavelength range of red diode laser arrays (630–690 nm) and emission bandwidths comparable to that of Ti:sapphire ( $\sim 220$  nm), are of special interest. At first sight, Cr:LiSGaF and Cr:LiSAF are very similar with respect to basic spectroscopic properties [5] and therefore should exhibit similar lasing and ultrashort-pulse operation characteristics. However, comparing the performance

of Cr:LiSAF and Cr:LiSGaF in the same resonator configuration (conventional astigmatically compensated X-cavity), one should note that Cr:LiSGaF demonstrates higher output power in cw (900 mW) and in mode-locked (200 mW) operation than Cr:LiSAF [5]. In the Q-switched regime, Cr:LiSGaF produced four times more energy (12  $\mu$ J at 10 kHz repetition rate) than Cr:LiSAF under the same conditions [6]. Based on these considerations, we anticipate that the application of the concept, recently suggested in [7], to Cr:LiSGaF, allowing for the better diode-pump-resonator beam mode-match and thus higher output power (1.1 W in Cr:LiSAF, the highest value achieved up to now in cw-regime), would also enable even higher cw output powers. In any case, we believe that Cr:LiSGaF, along with the well-established Cr:LiSAF crystal, coupled with advances in 670 nm GaInP/AlGaInP diode lasers and in chirped dielectric mirror technology, offers the potential for the most compact all-solid-state femtosecond laser sources in the future. At this point it is worth stressing that not only the semiconductor pump source but also the prismless dispersion compensation design essentially contributes to the compactness of the laser. In this paper and at this stage of research, we concentrate on the latter aspect, keeping in mind the possibility of a combination of a prismless resonator design with diode-pumping at the very next stage.

Nowadays Kerr-lens mode-locked (KLM) Cr:LiSAF (e.g., [8–10]) and Cr:LiSGaF lasers [5, 11–13] routinely produce pulses below 50 fs [9, 14–19]. However, the shortest pulses obtained in Cr:LiSAF lasers (18 fs [15] and 24 fs [16]) were achieved at the expense of the output power which is negligible in both cases, and at the expense of pulse quality, i.e., which has a relatively large ( $> 0.4$ ) time-bandwidth product.

Recent achievements in the technology of compact mirror dispersion controlled (MDC) ultrashort pulsed Ti:sapphire lasers generating around- and sub-10 fs pulses ([20–23]) stimulated recent research, which aims towards the development of similar performing chirped mirror dispersion controlled Cr:LiSGaF and Cr:LiSAF lasers. However, this task has remained unsolved at the first stage. This is mainly due to

an order of magnitude lower gain in the  $\text{Cr}^{3+}$ -doped materials in comparison to that in Ti:sapphire and correspondingly lower tolerance to relatively high losses ( $\sim 0.3\%$  per reflection) introduced by the chirped mirrors (CM) of the first generation [24]. Besides, owing to the lower thermal conductivity and the presence of upconversion in these crystals, one has to work with low doped (Cr-concentration should be kept below 1.5–2% [5] in order to avoid upconversion losses and win in the output power) and therefore relatively long crystals. Typically, the length of these crystals is a few mm as compared to 1.5–2 mm in Ti:sapphire, thus leading to the necessity of compensating for more material dispersion. In order to provide the necessary dispersion compensation (even though it is lower than in Ti:sapphire), a larger number of reflections from dispersive mirrors is required. This increases the intracavity losses, which become larger than the maximum small-signal gain, making laser action practically impossible.

In order to solve the described problem, we suggested another type of dispersive dielectric mirror in the form of the Gires–Tournois (GT) interferometers for intracavity dispersion control in KLM Cr:LiSGaF lasers [19, 25]. In fact, the first prismless diode-pumped Cr:LiSAF laser based on a semiconductor saturable absorber mirror (no KLM action) with GT-type coating was realized by Kopf et al. [26, 27], which produced 160 fs pulses at 25 mW output power. Soon after, we demonstrated the first prismless  $\text{Kr}^{+}$ -pumped KLM Cr:LiSGaF laser [19, 25], with low-loss GT structured dielectric mirrors replacing conventional cavity mirrors. This laser produced stable, reproducible 44 fs pulses at 200 mW of output power [19]. GT mirrors (GTM) have the advantage of negligibly low intrinsic loss, and relatively high and adjustable negative GDD. In this work we report the further shortening of the pulses down to 37 fs at the expense of output power (100 mW), which indicates that we approached the ultimate limits achievable with GTMs.

Opposite to GTMs, chirped mirrors (CM) exhibit nearly constant GDD over a much larger bandwidth than can be obtained by using GTMs for dispersion control. It was a challenging task to improve the technology of dielectric chirped mirrors in order to make them suitable for the lower gain Cr:LiSAF and Cr:LiSGaF lasers as compared to Ti:sapphire lasers. This has been successfully accomplished recently, and novel low-loss chirped mirrors, differing from the old generation of chirped mirror through its design and new evaporation materials, could be manufactured [24, 28].

In this paper, we describe the state of the art of MDC Cr:LiSGaF/Cr:LiSAF lasers. Both crystals were of comparable good quality ( $\sim 0.1\%$ /cm scatter loss). Sub-20 fs pulses with relatively high average output power (up to 100 mW in Cr:LiSGaF and 50 mW in Cr:LiSAF) were generated in both types of lasers. We present analysis of the optimization of the MDC KLM Cr:LiSGaF and Cr:LiSAF oscillators, operating with both hard and soft apertures. We also discuss phenomena that accompany pulse formation connected with higher-order dispersion, as well as the effect of a red shift in the operating wavelength, observed at shorter pulse durations. Comparing the advantages and drawbacks of each type of laser (GTM or CM dispersion controlled), we are trying to circle out application areas for each of them. Finally, we analyze the potential of the present setup, based on CMs, and try to determine whether sub-10 fs pulse generation is feasible in this type of laser.

## 1 Experimental setup

### 1.1 Gires–Tournois vs. chirped mirrors: Advantages and drawbacks

Basically, two types of dispersive dielectric mirror are known to be implemented at the moment: Gires–Tournois interferometers [29, 30], which are essentially étalons, and chirped dielectric mirrors [24, 31]. The first suggestions for the compression of chirped optical pulses by means of interferometer-like structures go back to 1964 [32, 33]. Enhanced interest toward dielectric cavity-mirror dispersion compensation evolved in connection with colliding-pulse mode-locked cw dye lasers in the middle of the 1980's. However, at that time, such mirrors failed to support pulses shorter than 50 fs [29, 34]. Based on this idea, the technology of GT structured dispersive dielectrical mirrors has been recently developed [19, 24]. On the one hand, GTMs have the advantage of negligible transmission loss, and relatively high and adjustable (via change of the angle of incidence) group delay dispersion, thus being well suited for intracavity applications in femtosecond lasers. On the other hand, the bandwidth of the parabolic dispersion curve of GTMs is limited to a few tens of nm, hence making the generation of sub-20 fs pulses practically impossible. The other candidate for non-prismatic dispersion compensation, i.e., chirped mirrors, exhibits nearly constant group delay dispersion (GDD) over a much larger bandwidth (typically 100–200 nm) than can be obtained by using GT interferometers.

In Fig. 1 we compared the group delay and GDD of a chirped mirror and of a GT interferometer. The dispersion of the GT structure may surpass that of the chirped mirror, with both designed for 850 nm as a central wavelength (Fig. 1). However, the chirped mirror exhibits about a 50% higher group delay per reflection. It has been shown in [35] that in the case of dielectric high reflectors the losses in the layers are proportional to the group delay per reflection, when we assume absorption and scattering in the dielectric layers to be frequency and material independent. Based on this consideration, we expected at least a 30% reduction of intracavity losses when using GT-type mirrors. Indeed, we observed the scattering loss of less than 0.1% (vs. 0.1–0.3% in CMs) and negligible transmission loss ( $< 0.01\%$  vs. 0.2–0.4% in CMs), which was actually even lower than in the high-reflective mirrors used by us.

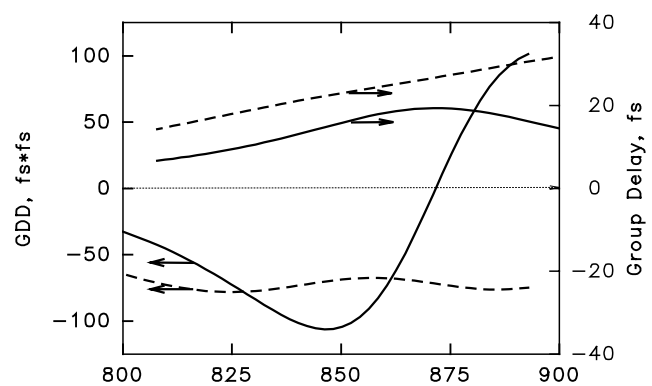
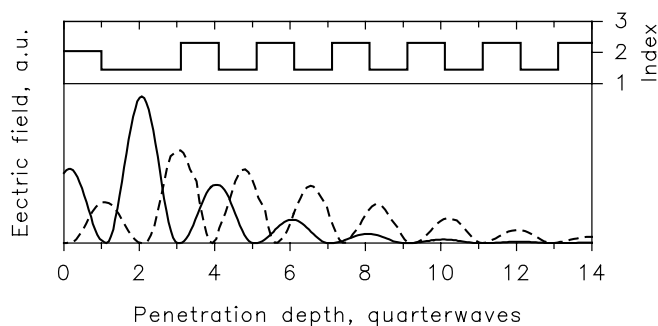


Fig. 1. Comparison of GDD and group delay per reflection of GT mirrors (solid line) and chirped mirrors (dashed lines)



**Fig. 2.** Comparison of electrical field distribution within GT mirror (*solid line*) and chirped mirror (*dashed lines*). Inset shows index of refraction change within the GT structure

An additional advantage of GT structures with respect to the losses is that the electric field can easily be concentrated in the low refractive index material placed in the spacer region (Fig. 2) which has lower losses than high-index materials.

Dispersion of the Gires–Tournois and the low-loss chirped mirrors has been measured by the spectrally resolved white-light interferometer technique described in [36]. We found however that this method cannot be easily applied to measuring the dispersion of the laser crystals since the plane wave approximation we used earlier is not valid, mainly because of the relatively poor flatness of the used crystal sample surfaces.

Therefore, we adopted the measurement arrangement of Sainz et al. [37,38], which requires practically the same measurement apparatus but is not sensitive to the problems mentioned above.

There are two main differences in the two methods: (i) in Sainz’s arrangement, the mirrors of the Michelson interferometer are set parallel, while in the other set-up, one of the mirrors is tilted around a horizontal axis; (ii) for evaluation of the experimental data, only one horizontal line of a 2D CCD array has to be used in Sainz’s arrangement, whose data is not affected by the poor quality of the crystal surface. In our practice, we measured the group delay of the crystal rather than the retrieved phase [37] by measuring the change in the periodicity of the spectrally resolved interferometric pattern, which is just the inverse of the group delay when the period is expressed in angular frequency units ( $\omega = 2\pi c/\lambda$ ). The accuracy of Sainz’s method was found to be much lower than in the arrangement published in [36], which can easily be explained by the much higher number of data points processed in the latter technique. Details of the technique will be published elsewhere [39].

Reliability of our dispersion measurement on the crystal has been experimentally verified by measuring the dispersion of the GT mirrors by using both Sainz’s [37] and Bor’s [36] arrangement. The measured GD and GDD values were the same within the error bar of the data obtained by the former arrangement. The measured dispersion of a Cr:LiSGaF crystal is shown in Fig. 3. Our assumptions were experimentally verified by reflectance measurements on the mirrors. We found that reflection losses are proportional to the measured group delay functions of the mirrors: 5 fs group delay per reflection corresponds to  $\approx 0.2\%$  of scattering loss.

Two sets of chirped mirrors have been tested consecutively in the process of working out of the technology of

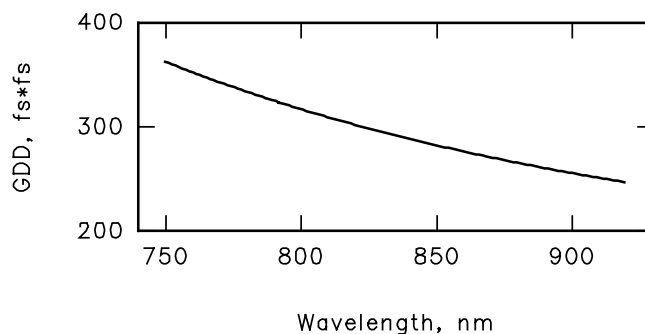


**Fig. 3.** GDD per centimeter of a LiSGaF crystal

novel low-loss mirrors. The first fabricated set exhibited unacceptably high losses of 0.2–0.3% per reflection and therefore could hardly be employed successfully. The second set was considerably improved in this respect with 0.1–0.2% losses.

Using the measured dispersion data for the mirrors and for the crystals, we optimized the net GDD of the resonator (Fig. 4). It can be seen that the overall GDD is still far from approaching the zero line. This can be partially explained by our observation that in the presence of excessive negative GDD, the pulses tend to be more stable than in a completely optimized regime.

Finally, let us summarize the advantages and the drawbacks of GT and CMs. In the case of GT mirrors, the advantages are negligible transmission loss, lower group delay than in CMs and hence lower scattering losses, and higher and adjustable (by tuning the angle of incidence) GDD. The obvious drawback is the unavoidable presence of higher-order dispersion, which may easily lead to sideband generation and pulse splitting [40], unless special care is taken to avoid these effects. In the case of CMs, the major advantage is the broader (and constant) useful bandwidth at the expense of lower GDD and higher losses. Expanding on this, the following application areas may be circled out for GT MDC lasers: they could form a source for tunable 50–100 fs pulses of appreciable output power for many “real-world” applications in physics, medicine, chemistry, and biology. Researchers in-

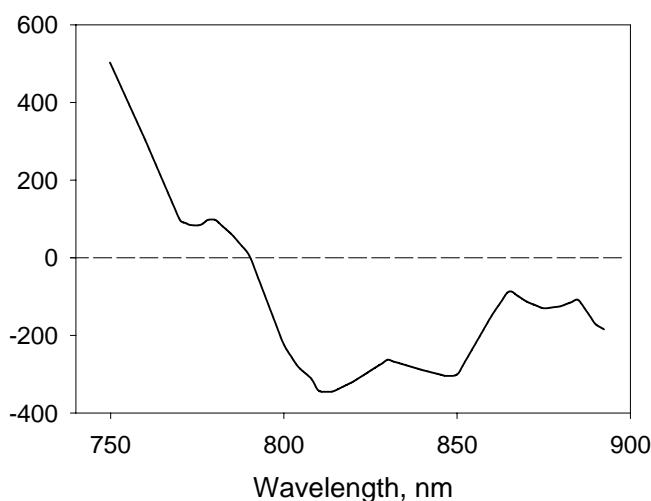


**Fig. 4.** Net GDD per round-trip in a CM dispersion-controlled laser oscillator

terested in investigating various ultrafast phenomena would naturally prefer a sub-20 fs MDC laser source.

### 1.2 Resonator design

The relatively low nonlinear index of refraction of Cr:LiSAF and Cr:LiSGaF [8] and the necessity to minimize the negative GDD to obtain shorter pulses both tend to increase the starting threshold of the mode-locked operation and reduce pulse stability. We found experimentally that the resonator designs suggested for Ti:sapphire lasers, e.g., in [41,42] are suitable for Cr:LiSGaF lasers with relatively high negative GDD and correspondingly long pulses, e.g., in prism- and GTI-mirror-controlled lasers [5, 19], but did not provide enough self-amplitude modulation (SAM) with optimized GDD. We therefore performed a theoretical analysis, aimed toward achieving the highest possible SAM and resulting in a cavity design different from those previously suggested.

In all realized laser oscillators, we used a generic X-folded cavity (see Fig. 5) with two curved (radius of curvature 100 mm) folding mirrors, output coupler varying from 0.4 to 2.3%, and dispersive mirrors in different combinations.

The optimization of the cavity for KLM has been performed on the basis of paraxial Gaussian beam approximation. Outside of the nonlinear crystal, we used the ABCD matrix formalism, while the nonlinear propagation was treated in the first-order aberrationless approximation. This approach has been successfully used for the Ti:sapphire oscillators [41–43] and found to be quite satisfactory for explaining experimental observations.

Our main parameter of interest is the small-signal SAM at the aperture inside the resonator, which is proportional to the modulation coefficient

$$\delta_{SAM} = \left( \frac{1}{w} \frac{dw}{dp} \right)_{p=0}, \quad (1)$$

where  $w$  is the spot size,  $p = P_{ic}/P_{crit}$  is the normalized power,  $P_{ic}$  is the instantaneous intracavity power, and  $P_{crit}$  is the critical power for self-focusing  $P_{crit} = \lambda^2/2\pi n n_2$ , where  $\lambda$  is the wavelength in vacuum,  $n$  is the linear, and  $n_2$  is nonlinear refractive indices, respectively. Taking typical values for Cr:LiSGaF and Cr:LiSAF ( $\lambda = 860$  nm,  $n = 1.4$ , and  $n_2 \approx 8 \times 10^{-17}$  cm<sup>2</sup>/W [44]), we obtain  $P_{crit} = 10$  MW, which is about 6 times higher than  $P_{crit}$  in Ti:sapphire.

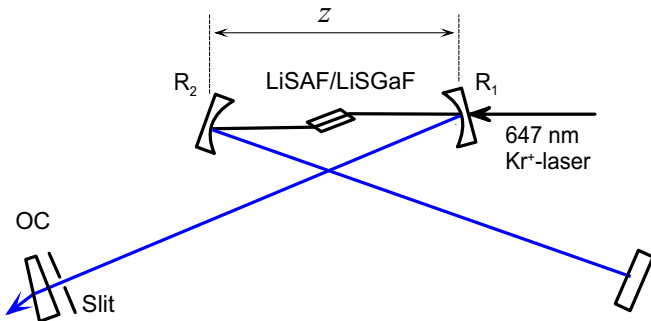


**Fig. 5.** Generic scheme of the experimental setup. OC, output coupler, varying between 0.4 and 2.3%;  $z$ , optical distance between folding mirrors;  $R_1$ ,  $R_2$ , radii of curvature. Optional flat dispersive mirrors not shown

To find the most favourable resonator configuration (with highest *negative* value of the SAM coefficient), we computed  $\delta_{SAM}$  for the whole stability range and physically reasonable crystal displacements.

The results for the anastigmatic case are plotted both for the asymmetrical (Fig. 6) and the symmetrical cavity arrangements (Fig. 7), taking crystal length  $l_{cryst} = 5$  mm, radii of curvature of the folding mirrors 100 mm, and typical experimental arm lengths. The stability variable  $z'$  is equal to  $z' = z - (R_1 + R_2)/2$  (see Fig. 5) and is normalized by the width of the stability range  $S$ , while the crystal displacement  $x$  is nor-

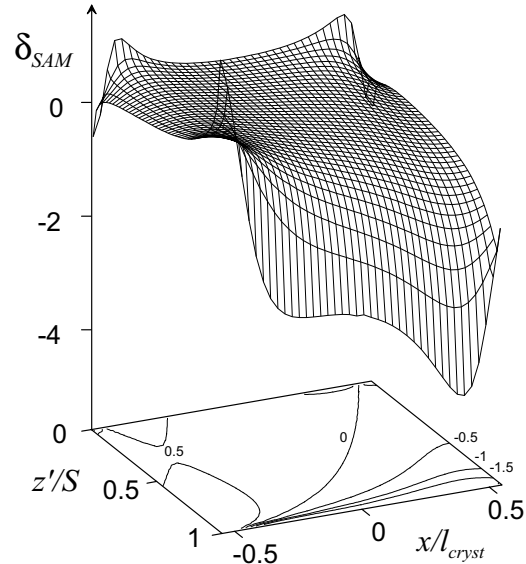


**Fig. 6.** Plot and corresponding contour-line diagrams of the SAM coefficient  $\delta_{SAM}$  vs. normalized stability parameter and relative crystal displacement. Asymmetrical cavity with arm lengths of 87 and 109 cm. Positive values of  $x$  correspond to displacement towards the shorter arm containing the slit

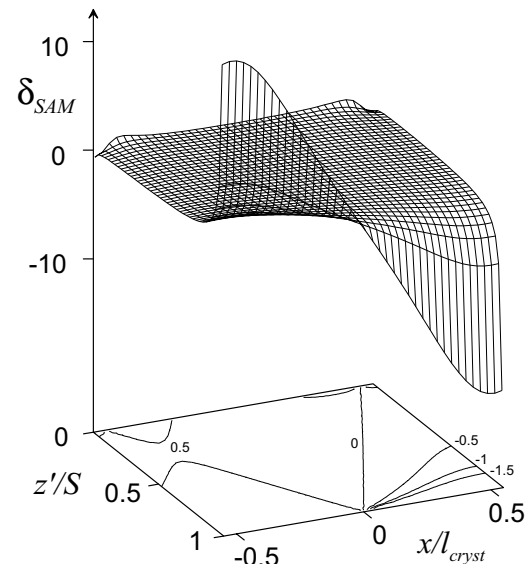


**Fig. 7.** Plot and corresponding contour-line diagrams of the SAM coefficient  $\delta_{SAM}$  vs. normalized stability parameter and relative crystal displacement. Symmetrical cavity with arm lengths of 95 cm. Positive values of  $x$  correspond to displacement towards the arm containing the slit

malized by the crystal length  $l_{\text{cryst}}$ . The important distinction of the plots in Figs. 6 and 7 from those published in the literature [42, 43, 45] is that the crystal position is measured as a displacement of the crystal center from the waist location, rather than quite an abstract distance from one of the mirrors. The beam waist radius and its position relative to the crystal faces completely define the nonlinear interaction of the beam with the crystal. Making additional use of the normalized coordinates thus leaves only the asymmetry of the cavity and  $l_{\text{cryst}}/S$  ratio as independent parameters. In practical terms, the plots in Figs. 6 and 7 represent all relevant features of an arbitrary X-folded cavity. Consistent with previous publications [43, 45], these plots predict that it is possible to obtain higher values of SAM in the symmetrical configuration. However, these maximum values are obtained at crystal displacements approaching  $x/l_{\text{cryst}} = \pm 0.5$ , i.e., when the beam waist lies at the crystal surface. This means that in order to make use of the high SAM in this configuration, the beam waist must be shifted in the crystal toward one of the surfaces, away from the optimal position. On the contrary, even a slightly asymmetric cavity exhibits an extended region of relatively high SAM coefficient at crystal displacement around zero, i.e., including the optimal configuration.

Both Figs. 6 and 7 show only the first stability range. It is possible to show that within the anastigmatic approximation, the SAM coefficient function in the second stability range is always a centrosymmetrical image of the first stability range. The center of symmetry is located in the middle of the stability gap with crystal displacement equal to zero. Moreover, this result is valid also for the astigmatic cavity, provided that every folding mirror compensates one half of the crystal length and that the exact compensation is done for the middle of the stability gap. This implies that KLM action should be equally easy to obtain in both stability ranges. In practice, however, we found that most stable pulses are obtained in the second stability range, where hard-aperture KLM is substantially aided by the soft-aperture KLM action. Contrary to the hard-aperture KLM, soft-aperture KLM behaves differently in the two stability ranges even in the anastigmatic approximation and reaches appreciable values only in the second stability range [46]. The laser may also be mode-locked using the soft-aperture mechanism alone, but in this case, the mode-locking behaviour is almost uncontrollable and output mode quality is rather poor.

Taking into account all the above considerations, we believe that the optimal configuration is a slightly asymmetric cavity, operated in the second stability range. The most favorable mode of operation is the combination of soft and hard aperture KLM.

## 2 Experimental results and discussion

In the experimental setup described above we realized both the soft and hard aperture KLM. The self-mode-locked operation was initiated by moving the output coupler either manually or with the help of a piezoelectric driver.

### 2.1 GTI-based Cr:LiSGaF laser

As a first step, we replaced the prism pair of a former X-cavity resonator [5] by a multiple-reflection GTM pair so that the

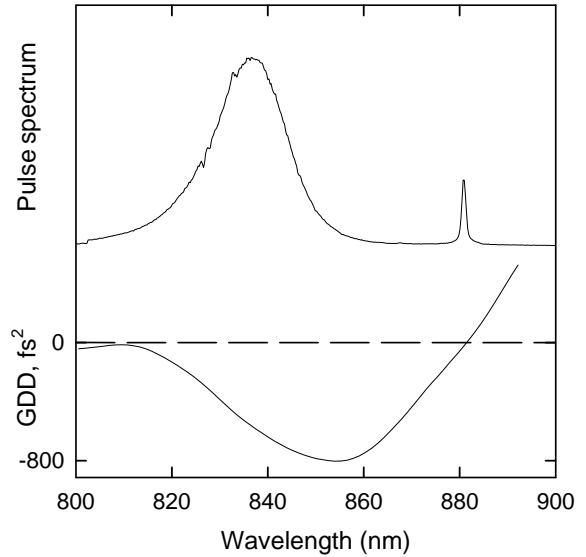


**Fig. 8.** Spectrum of the mode-locked GTM dispersion-controlled laser and calculated net GDD per round-trip

calculated amount of GDD was at least as high as that of the prism pair. This required 6 reflections of  $\approx -50 \text{ fs}^2$  per bounce. The laser could be mode-locked, achieving  $\approx 50 \text{ fs}$  pulse duration. The typical spectrum of the mode-locked laser is shown in Fig. 8. Assuming a  $\text{sech}^2$  pulse shape, we obtained a pulse length of 47 fs from the interferometric auto-correlation, corresponding to a  $\Delta\tau\Delta\nu$  product of  $\approx 0.33$ . The interesting characteristic feature of the pulse spectrum is the presence of a narrow side-band around  $\lambda = 880 \text{ nm}$ . Using the measured GDD of the Cr:LiSGaF crystal and the calculated GDD of GTMs at actual angles of incidence, we were able to calculate the overall net GDD of the resonator per round-trip. Since the measured GDD of the GTMs at normal incidence followed the theoretical curve very closely, use of the calculated GDD at oblique incidence is justified. Comparison of both curves in Fig. 8 shows that the side-band occurs close to the position of the spectrum, where the GDD function crosses the zero line, while the third-order dispersion (TOD)  $D_3$  is relatively high. Under this perturbative influence of the TOD, a strong resonance peak may develop in the spectrum. The frequency shift from the central frequency of the pulse in this case should also satisfy the phase-matching condition [47]:

$$\Delta\omega^2 + \frac{D_3}{3D}\Delta\omega^3 = -\frac{1}{T^2}, \quad (2)$$

where  $D$  is the second-order dispersion,  $T = \tau/1.76$ , and  $\tau$  is the solitary pulse duration. The calculated  $\Delta\omega$  corresponds within measurement accuracy to the experimentally observed value. This provides strong evidence for the assumption that the side-band originates from nonlinear energy dissipation of the solitary pulse due to the TOD perturbation. Experimentally, the dispersive wave could be suppressed by either increasing the self-amplitude modulation (closing the slit) or modifying the net GDD of the laser to avoid the resonance condition (2) close to the pulse spectrum.

However, the high number of GT reflections in the above experiment introduced appreciable losses into the cavity, so that the maximum output power was limited to 100 mW. Since we measured the transmission through the GT mirrors

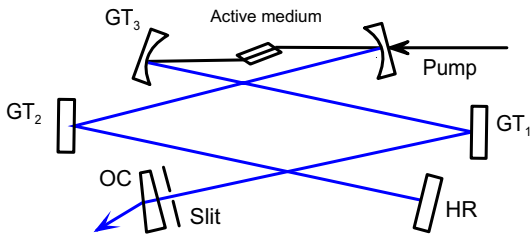


**Fig. 9.** Schematic of the KLM Cr:LiSGaF laser with GT mirrors replacing resonator mirrors. OC, output coupler; GT, Gires–Tournois mirrors; HR, high reflector

to be below 0.01%, less than that of our conventional high reflector ( $\approx 0.02\%$ ), we attribute the additional losses ( $\approx 0.1\%$  per bounce) to scattering, as described above.

Therefore, we attempted to reduce the number of reflections to a minimum, by combining GT mirrors produced with different technologies and nominal GDD. Our final laser design is shown in Fig. 9 and incorporates 3 GT mirrors, one of them being curved. This design is characterized by its compactness and excellent long-term alignment stability. With this laser, we routinely reproduced mode-locked operation at pump powers of 1.5–1.8 W from a Kr-ion laser at 647 nm (0.95–1.15 W absorbed in the crystal) and mode-locked output powers of 150–200 mW with 2.3% output coupling. Pulse durations were typically 45–50 fs, with the shortest measured pulse duration being 44 fs (Fig. 10). The pulses were nearly transform-limited, with a time-bandwidth product of  $\Delta\nu\Delta\tau \approx 0.33$ –0.36. By varying the angles of incidence at the flat GT mirrors between  $5^\circ$  and  $20^\circ$  and choosing different GT mirror combinations it was possible to tune the central wavelength between 833 and 857 nm. In Fig. 11 the values of the pulse lengths are plotted; they were obtained in the resonator with 2.3% OC and depend upon the operation wavelength. Although the variation in the pulse duration is minimal, one can see a clear tendency for the pulses with shorter durations to operate near the maximum of the gain spectrum. With the repetition rate being approximately 80 MHz, the output and intracavity pulse energies were found to be 2.5 nJ and 110 nJ, respectively.

We found that increasing the intracavity pulse energy above 100–110 nJ was often accompanied by a reproducible double-pulse oscillation regime, with typical pulse separation

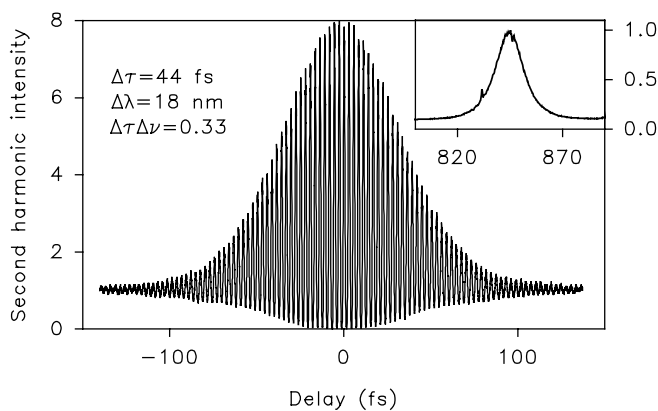


**Fig. 10.** Autocorrelation trace of a mode-locked Cr:LiSGaF laser. The inset shows the output spectrum

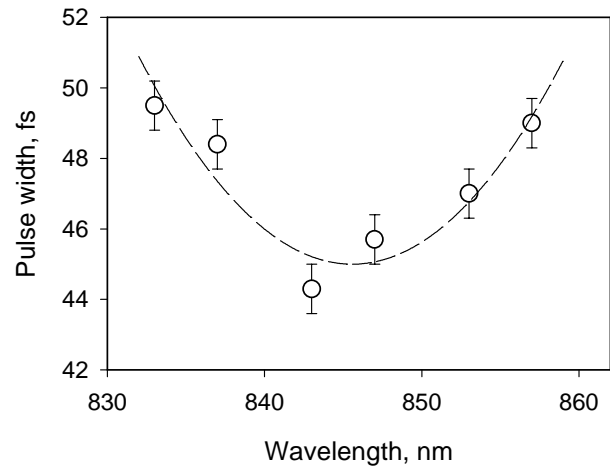


**Fig. 11.** Pulsewidth vs. wavelength in a GTM dispersion-controlled laser. The laser was tuned by changing the angle of incidence upon the GTMs. Dashed line is an eye-guide

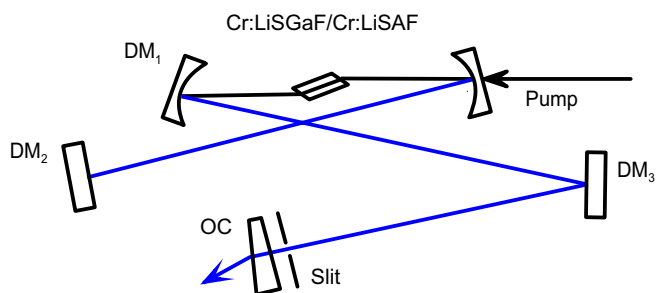


**Fig. 12.** Mirror dispersion-controlled Cr:LiSGaF (Cr:LiSAF) laser. OC, output coupler; DM, dispersive mirror, either GT-type or chirped (see text)

300–500 fs. Both pulses appeared to be more or less identical and the separation stable over indefinite time. Theoretical analysis of this phenomenon in solid-state lasers was very recently given in [40]. To suppress this double-pulse regime, it was necessary to decrease slit width, increase the SAM, and reduce the output power, eventually bringing the intracavity pulse energy below 100 nJ.

Further optimization of the resonator and the active medium led to a simplification of the laser cavity, which finally yielded the simple five-mirror X-cavity shown in Fig. 12, with all but the output coupler and dichroic pump coupler mirrors providing dispersion compensation. The pulses, produced in such a scheme, were nearly transform-limited 37 fs pulses with a time-bandwidth product of 0.34 and an output power of about 100 mW. These pulses are obviously limited by the GDD bandwidth of GTMs and are the shortest pulses ever achieved with GT mirrors. Further reduction of the pulse duration is only possible with broadband chirped mirrors.

## 2.2 Chirped MDC Cr:LiSGaF and Cr:LiSAF lasers

In order to achieve the broader and flatter dispersion spectrum, we first used a combination of chirped and GT mirrors. The laser could be easily mode-locked, with a  $\text{sech}^2$  pulse shape fit to the measured autocorrelation trace, yielding a pulse length of 33 fs and a time-bandwidth product

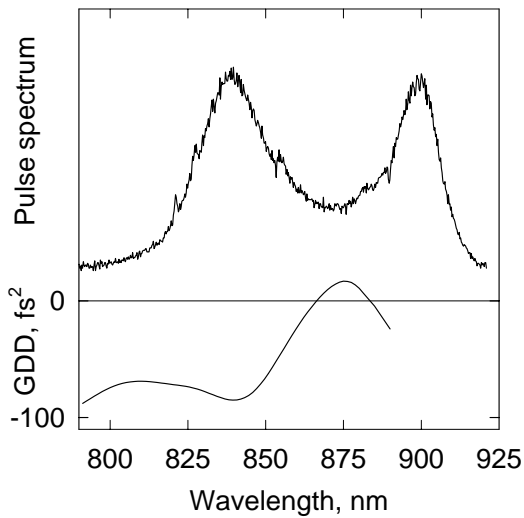


**Fig. 13.** Measured GDD spectrum (*lower curve*) of the first version of the low-loss chirped mirrors designed for Cr:LiSAF and Cr:LiSGaF lasers and spectrum (*upper curve*) of the mode-locked pulses obtained by using these mirrors

of  $\Delta\tau\Delta\nu = 0.4$ . The losses in the chirped mirrors were low enough to allow a mode-locked output power of up to 90 mW at 1 W of absorbed pump power. As can be seen, this pulse duration far from fully exploits the available bandwidth of the active medium. The non optimized dispersion curve of the first chirped mirrors for Cr:LiSAF and Cr:LiSGaF effectively cut a substantial part of the gain spectrum in its infrared part (Fig. 13).

The curious form of the dispersion curve showing positive values at  $\lambda$  around 870 nm and becoming negative again at 885 nm caused the double-peaked pulse spectrum, corresponding to a modulated autocorrelation trace with accompanying sidelobes (Fig. 14). This resembles the recently reported double-peaked pulses [48–50], generated in prism dispersion controlled Ti:sapphire lasers. In the latter case the dip in the center of the spectrum was explained by the positive dispersion at 850 nm, implying worse conditions for mode-locking near the center of the spectrum [50]. Similar situ-

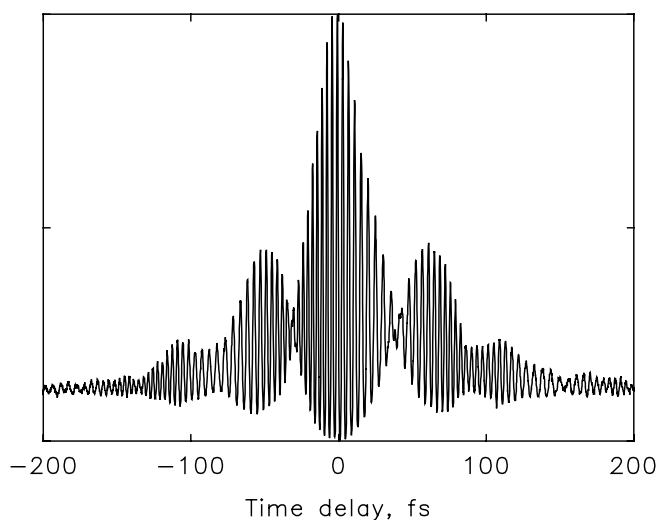


**Fig. 14.** Autocorrelation trace, corresponding to the spectrum in Fig. 13

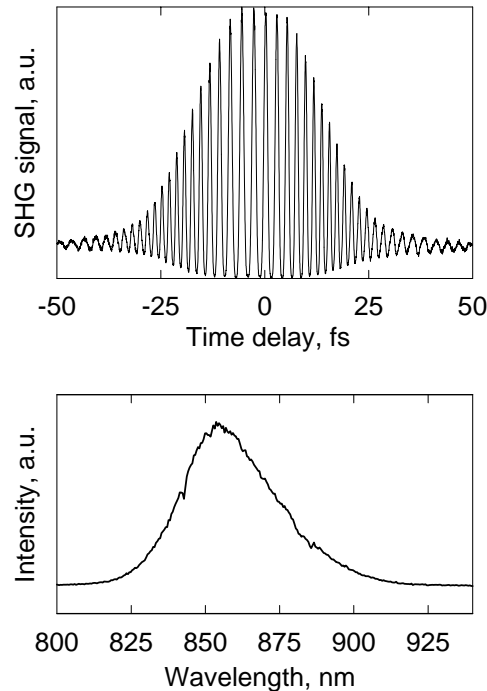


**Fig. 15.** Interferometric autocorrelation trace and spectrum of 24 fs pulses from a mode-locked Cr:LiSAF laser, using an improved version of chirped mirrors

ation takes place in our case, when the optimum conditions for mode-locking are being achieved symmetrically around the maximum of the mirror GDD spectrum, i.e., at 840 and 900 nm. Rough estimations of the observed effective bandwidth allowed the conclusion that proper dispersion compensation provided by improved chirped mirrors would even support the generation of sub-20 fs. The optimization of the dispersion of the CM and of the overall GDD of the resonator has led to the actual realization of sub-20 fs pulse durations of both Cr:LiSAF and Cr:LiSGaF lasers. Mode-locked operation of both lasers was compared in the same resonator. The typical pulses obtained in the Cr:LiSAF laser are 24 fs long (Fig. 15) and have an output power of 60 mW with 2.3% output coupling at about 800 mW of absorbed pump power, and a time-bandwidth product of  $\Delta\tau\Delta\nu = 0.36$ . In the Cr:LiSGaF laser, even shorter pulses (18 fs) (Fig. 16a) were obtained with 0.9% output coupling at 100 mW output power and 1.1 W of absorbed pump power with a time-bandwidth product of  $\Delta\tau\Delta\nu = 0.33$ . The shorter pulse duration in Cr:LiSGaF may be explained by the operation of this laser at a higher intracavity power and relatively smaller net GDD in this case. In order to raise the intracavity power in the Cr:LiSAF laser, we reduced the output coupling down to 0.4% and increased the absorbed pump power to 1.08 W. In this way, 19 fs pulse duration could be achieved also in a Cr:LiSAF laser, however, at the expense of output power (50 mW) and an increased time-bandwidth product of  $\Delta\tau\Delta\nu = 0.44$  (Fig. 16b).

The feasibility of sub-20 fs pulses generation in Cr<sup>3+</sup>-doped materials, without sacrificing output power and pulse quality, determines the challenging task of approaching the values, which is typical for Ti:sapphire systems. In order to estimate the limitations of present systems, we made a plot of generated pulsewidths vs. amount of net intracavity GDD (Fig. 17). According to the theory [51], pulse width should

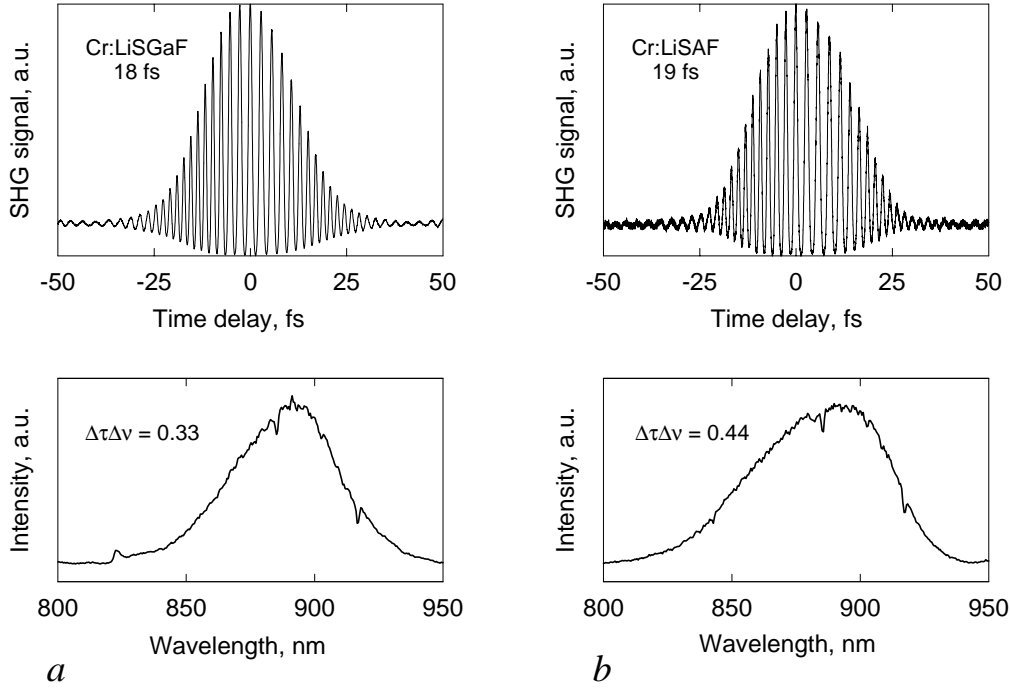


**Fig. 16a,b.** Interferometric auto-correlation traces and spectra of sub-20 fs pulses from Cr:LiSGaF and Cr:LiSAF lasers, containing an improved version of chirped mirrors.

**a** Cr:LiSGaF laser, pulse width 18 fs, output power 100 mW;  
**b** Cr:LiSAF laser, pulse width 19 fs, output power 50 mW

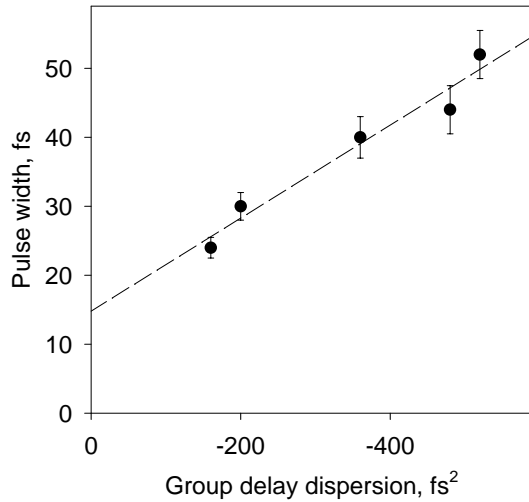


**Fig. 17.** Pulse width in Cr:LiSAF vs. net intracavity GDD. All measurements have been made in the same setup (0.9% output coupling)

linearly depend upon the residual amount of second-order dispersion:

$$\tau = \frac{3.53|D|}{\phi W} + \alpha\phi W, \quad (3)$$

where  $\phi$  is a maximum phase shift due to self-phase modulation,  $W$  is pulse energy,  $D$  is the net negative second-order dispersion, and  $\alpha$  is a coefficient in the range of 0.1–0.3, depending upon the position at which the pulse is extracted from the cavity. For the cavities with symmetrized dispersion,  $\alpha$  is close to its lower value at the ends of the resonator. Comparison of this expression with Fig. 17 suggests that in our setup, optimization of the GDD alone may lead to pulsewidths of about 15 fs in Cr:LiSAF and probably even

less with Cr:LiSGaF. Further pulse shortening would require control of higher-order dispersion as well as an increase of the bandwidth of the CMs. Currently, although the CM losses have been dramatically decreased, we still had to trade bandwidth with GDD to achieve the lowest possible number of reflections. We believe that advances in mirror-coating technology will allow the use in Cr<sup>3+</sup>-based systems of CMs with the same bandwidths as is now possible in Ti:sapphire lasers. Another simple estimation shows that at a 70 MHz repetition rate and 10 W of average intracavity power, the 18 fs pulse has peak power of 8 MW, close to the above-mentioned  $P_{\text{crit}}$ . The laser is operating in the regime of strong nonlinear spatial-temporal interaction[52], typical for sub-20 fs Ti:sapphire lasers. We therefore see no fundamental obstacles to approaching the 10-fs barrier.

Another interesting phenomenon, which was observed in these experiments, is the reproducible infrared shift of the operational wavelength, when pulse duration approaches 20 fs mark (see Fig. 16). This effect can be observed in both Cr:LiSAF and Cr:LiSGaF crystals. For comparison,  $\sim 40$ – $50$  fs pulses are centered spectrally around 850 nm, i.e., around the maximum of the gain curve. Looking at the corresponding spectra of the shortest pulses obtained in Cr:LiSAF [15, 16], one can easily see that in both references the operation wavelength lies between 870 and 880 nm. So far, three different groups have recorded this red-shift of the operational wavelength of pulses with durations close to 20 fs in Cr:LiSAF. It would be interesting to investigate further this finding in order to understand whether there is some fundamental physical mechanism that gives rise to this phenomenon, or whether it is a mere coincidence, and whether the shift occurs in each case for different reasons. At least in the prism-controlled resonator this can be explained by the fact that the third-order dispersion in fused silica becomes zero around 900 nm. However, if this red shift is due to a nonlinear effect in the active medium, then induced Raman scattering could be a possible explanation.

Finally, comparing the operation of a fused silica prism-pair controlled mode-locked laser and the MDC laser with the same amount of intracavity dispersion under similar conditions, we may conclude that in the sub-40 fs regime the latter demonstrates, according to our experience, much better pulse stability and higher pulse quality. As we understand, even a slight misalignment of cavity mirrors in a prism-containing resonator, caused, e.g., by the environmental perturbation, changes the in-glass optical distance, consequently influencing the pulse width, if not totally prohibiting mode-locking.

### 3 Conclusion

In conclusion, we described the state of the art of compact MDC Cr:LiSAF and Cr:LiSGaF lasers, producing high-quality sub-20 fs pulses with substantial average output power of 100 mW. We made the effort of optimizing the cavity by several considerations, heading finally towards the aim of realizing a really compact femtosecond MDC laser.

*Acknowledgements.* We gratefully acknowledge stimulating discussions with T. Brabec, F. Krausz, and Ch. Spielmann. This work was supported by the Austrian National Science Foundation Projects P10733-PHY and P11985-PHY, and by Gesellschaft für Mikroelektronik.

### Note added in proof

Recently we obtained 14 fs (100 mW) pulses in a simple four-mirror cavity.

### References

- D.E. Spence, P.N. Kean, W. Sibbett: *Opt. Lett.* **16**, 42 (1991)
- L.K. Smith, S.A. Payne, W.L. Kway, B.H.T. Chai: *IEEE J. Quantum Electron.* **28**, 2612 (1992)
- S.A. Payne, L.L. Chase, L.K. Smith, W.L. Kway, B.H.T. Chai: In *OSA Proc. on Adv. Sol.-State Lasers*, Vol. 10, (OSA, Washington, D.C. 1991) pp. 14–17
- S.A. Payne, L.L. Chase, L.K. Smith, W.L. Kway, H.W. Newkirk: *J. Appl. Phys.* **66**, 1051 (1989)
- I.T. Sorokina, E. Sorokin, E. Wintner, A. Cassanho, H.P. Jenssen, M.A. Noginov: *Opt. Lett.* **21**, 204 (1996)
- F. Balembois, F. Druon, F. Falcoz, P. Georges, A. Brun: In *Advanced Solid-State Lasers* (1997) Paper WD4-1
- D. Kopf, U. Keller, M.A. Emmanuel, R.J. Beach, J.A. Skidmore: *Opt. Lett.* **22**, 99 (1997)
- A. Miller, P. LiKamWa, B.H.T. Chai, E.W. van Stryland: *Opt. Lett.* **17**, 195 (1992)
- N.H. Rizvi, P.M.W. French, J.R. Taylor: *Opt. Lett.* **17**, 1605 (1992)
- P.M.W. French, R. Mellish, J.R. Taylor, P.J. Delfyett, L.T. Florez, *Electron. Lett.* **29**, 1262 (1993)
- I. Sorokina, E. Sorokin, E. Wintner, A. Cassanho, H.P. Jenssen: In *CLEO/Europe'94 Digest* (1994)
- I.T. Sorokina, E. Sorokin, E. Wintner, A. Cassanho, H.P. Jenssen, M.A. Noginov: in *Adv. Sol.-State Lasers*, Techn. Dig., (OSA, Washington, D.C. 1995)
- V.P. Yanovsky, F.W. Wise, A. Cassanho, H.P. Jenssen: *Opt. Lett.* **20**, 1304 (1995)
- M.J.P. Dymott, A.P. Ferguson: *Opt. Lett.* **20**, 1157 (1995)
- M.J.P. Dymott, A.I. Ferguson: In *CLEO*, (OSA, Washington, D.C. 1995)
- R. Mellish, N.P. Barry, S.C.W. Hyde, R. Jones, P.M.W. French, C.J. van der Poel, A. Valster: *Opt. Lett.* **20**, 2312 (1995)
- D. Kopf, K.J. Weingarten, L.R. Brovelli, M. Kamp, and U. Keller: In *CLEO*, Vol. 8 of *Techn. Dig.* (OSA, Washington, D.C. 1995) p. 252
- J.M. Evans, D.E. Spence, W. Sibbett, B.H.T. Chai, A. Miller: *Opt. Lett.* **17**, 1447 (1992)
- I.T. Sorokina, E. Sorokin, E. Wintner, A. Cassanho, H.P. Jenssen, R. Szipöcs: *Opt. Lett.* **21**, 1165 (1996)
- L. Xu, C. Spielmann, F. Krausz, and R. Szipöcs: *Opt. Lett.* **21**, 1259 (1996)
- A. Stingl, C. Spielmann, F. Krausz, and R. Szipöcs: *Opt. Lett.* **19**, 204 (1994)
- A. Stingl, M. Lenzner, C. Spielmann, F. Krausz, and R. Szipöcs: *Opt. Lett.* **20**, 602 (1995)
- A. Kasper, K.J. Witte: *Opt. Lett.* **21**, 360 (1996)
- R. Szipöcs, A. Kóházi-Kis: *Appl. Phys. B* **65** (1997)
- I.T. Sorokina, E. Sorokin, E. Wintner, A. Cassanho, H.P. Jenssen, and R. Szipöcs: In *Adv. Sol.-State Lasers* (OSA, San Francisco 1996)
- D. Kopf, G. Zhang, M. Moser, and U. Keller: In *CLEO* (OSA, Washington, D.C. 1995)
- D. Kopf, G. Zhang, R. Fluck, M. Moser, U. Keller: *Opt. Lett.* **21**, 486 (1996)
- I. Sorokina, E. Sorokin, E. Wintner, A. Cassanho, H. Jenssen, and R. Szipöcs: In *Advanced Solid-State Lasers Conference* (1997) Paper MF2-1
- J. Heppner, J. Kuhl: *Appl. Phys. Lett.* **47**, 453 (1985)
- P.M.W. French, C.F. Chen, W. Sibbett: *Opt. Commun.* **57**, 263 (1986)
- R. Szipöcs, K. Ferencz, C. Spielmann, F. Krausz: *Opt. Lett.* **19**, 201 (1994)
- F. Gires P. Tournois: *Compt. Rend. Acad. Sci. (Paris)* **258**, 6112 (1964)
- J.A. Giordmaine, M.A. Duguay, J.W. Hansen: *IEEE J. Quantum Electron.* **4**, 252 (1968)
- M. Yamashita, M. Ishikawa, K. Torizuka, T. Sato: *Opt. Lett.* **11**, 504 (1986)
- K. Ferencz, R. Szipöcs: *Opt. Eng.* **32**, 2525 (1993)
- A.P. Kovács, K. Osvay, Z. Bor, R. Szipöcs: *Opt. Lett.* **20**, 788 (1995)
- C. Sainz, P. Jourdain, R. Escaola, J. Calatroni: *Opt. Commun.* **110**, 381 (1994)
- V.N. Kumar and D.N. Rao: *J. Opt. Soc. Am. B*, **12**, 1559 (1995)
- R. Szipöcs, A.P. Kovács, Z. Bor: In *CLEO, paper CTuP32* (1997)
- J. Hermann, V.P. Kalosha, M. Müller: *Opt. Lett.* **22**, 226 (1997)
- T. Brabec, C. Spielmann, P.F. Curley, F. Krausz: *Opt. Lett.* **17**, 1292 (1992)
- V. Magni, G. Cerullo, S. de Silvestri: *Opt. Commun.* **101**, 365 (1993)
- V. Magni, G. Cerullo, S. De Silvestri, A. Monguzzi: *J. Opt. Soc. Am. B*, **12**, 476 (1995)
- A. Miller, P. LiKamWa, B.H.T. Chai, and E.W. van Stryland: *Opt. Lett.* **17**, 195 (1995)
- G. Cerullo, S. de Silvestri, V. Magni, and L. Pallaro: *Opt. Lett.* **19**, 807 (1994)
- M. Piché, F. Salin: *Opt. Lett.* **18**, 1041 (1993)
- J.N. Elgin: *Opt. Lett.* **17**, 1409 (1992)
- C. Spielmann, P.F. Curley, T. Brabec, F. Krausz: *IEEE J. Quantum Electron.* **30**, 1100 (1994)
- J. Zhou, G. Taft, C. Huang, M. Murnane, H. Kapteyn, I. Christov: *Opt. Lett.* **19**, 1149 (1994)
- I.P. Christov, M.M. Murnane, H.C. Kapteyn, J. Zhou, C.-P. Huang: *Opt. Lett.* **19**, 1465 (1994)
- T. Brabec, C. Spielmann, F. Krausz: *Opt. Lett.* **16**, 1961 (1991)
- I.P. Christov, H.C. Kapteyn, M.M. Murnane, C.-P. Huang, J. Zhou: *Opt. Lett.* **20**, 309 (1994)